

CROSS-SECTIONS FOR NEUTRAL-CURRENT NEUTRINO SCATTERING OFF ^{82}Se ISOTOPE

P.C. DIVARI

Department of Physical Sciences, Hellenic Army Academy
Vari 16673, Attica, Greece

(Received February 18, 2010)

In this paper we study the differential, integrated and total cross-sections for neutral-current neutrino scattering off $^{82}\text{Se}(\nu, \nu')^{82}\text{Se}^*$, using the Quasi-particle Random Phase Approximation (QRPA). As it is known this isotope plays a significant role in the NEMO double beta decay detector. Exploiting the obtained results, we investigate the response of this isotope as a supernova neutrino detector assuming a two parameter Fermi-Dirac distribution for the supernova neutrino energy spectra.

PACS numbers: 23.40.Bw, 21.60.Jz, 26.30.+k

1. Introduction

It is well known, that neutrinos and their interactions with nuclei have attracted a great deal of attention, since they play a fundamental role to nuclear physics, cosmology and to various astrophysical processes, especially in the dynamics of core-collapse supernova-nucleosynthesis [1–6]. Moreover, neutrinos proved to be interesting tools for testing weak interaction properties, by examining nuclear structure, and for exploring the limits of the standard model [7]. In spite of the important role the neutrinos play in many phenomena in nature, numerous questions concerning their properties, oscillation-characteristics, their role in star evolutions and in the dark matter of the Universe, *etc.*, remain still unanswered. The main goal of experimental [8–10] and theoretical studies [11–17] is to shed light on the above open problems to which neutrinos are absolutely crucial.

Among the probes which involve neutrinos, the neutrino-nucleus interaction possess a prominent position [18–24]. Thus, the study of neutrino scattering with nuclei is a good way to detect or distinguish neutrinos of different flavor and explore the basic structure of the weak interactions. Also, specific neutrino-induced transitions between discrete nuclear states with good quantum numbers of spin, isospin and parity allows us to study

the structure of the weak hadronic currents. Furthermore, terrestrial experiments performed to detect astrophysical neutrinos, as well as neutrino induced nucleosynthesis interpreted through several neutrino–nucleus interaction theories, constitute good sources of explanation for neutrino properties. There are four categories of neutrino–nucleus processes: the two types of charged-current (CC) reactions of neutrinos and antineutrinos and the two types of neutral-current (NC) ones. In the charged-current reactions a neutrino ν_l (antineutrino $\bar{\nu}_l$) with $l = e, \mu, \tau$, transforms one neutron (proton) of a nucleus to a proton (neutron), and a charged lepton l^- (anti-lepton l^+) is emitted as

$$\begin{aligned} \nu_l + (A, Z) &\longrightarrow l^- + (A, Z + 1)^* , \\ \bar{\nu}_l + (A, Z) &\longrightarrow l^+ + (A, Z - 1)^* . \end{aligned} \tag{1}$$

These reactions are also called neutrino (anti-neutrino) capture, since they can be considered as the reverse processes of lepton-capture. They are mediated by exchange of heavy W^\pm bosons according to the (lowest order) Feynman diagram shown in Fig.1 (a). In neutral-current reactions (neutrino scattering) the neutrinos (anti-neutrinos) interact via the exchange of neutral Z^0 bosons [see Fig.1 (b)] with a nucleus as

$$\begin{aligned} \nu + (A, Z) &\longrightarrow \nu' + (A, Z)^* , \\ \bar{\nu} + (A, Z) &\longrightarrow \bar{\nu}' + (A, Z)^* , \end{aligned} \tag{2}$$

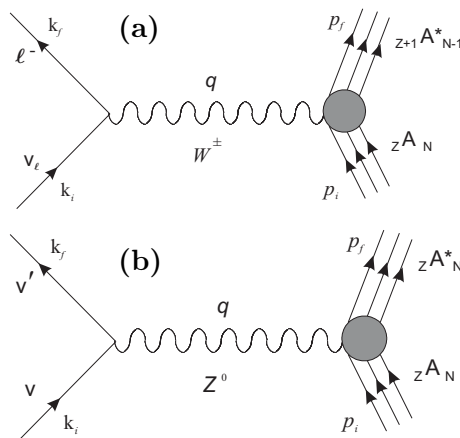


Fig.1. Feynman-diagram of lowest order for: (a) the CC neutrino–nucleus reactions $\nu_l + (A, Z) \longrightarrow l^- + (A, Z + 1)^*$, and (b) the NC neutrino–nucleus processes $\nu + (A, Z) \longrightarrow \nu' + (A, Z)^*$. The diagrams which correspond to the anti-neutrino reactions are similar.

where ν ($\bar{\nu}$) denote neutrinos (anti-neutrinos) of any flavor. The neutrino–nucleus reactions leave the final nucleus mostly in an excited state lying below particle-emission thresholds (semi-inclusive processes) [15]. The transitions to energy-levels higher than the particle-bound states usually decay by particle emission and, thus, they supply light particles that can cause further nuclear reactions.

Recently, it became feasible to detect low-rate neutrinos by measuring the recoiling nucleus with very-low threshold-energy gaseous-detectors. Such studies are in conjunction with the direct-detection of cold dark matter (CDM) events and double beta decay measurements. As it is well known, double beta decays are rare nuclear decays, mediated by exchange of a virtual neutrino between two nucleons in a nucleus, sensitive to the Majorana neutrino mass, the right-handed neutrino and to other neutrino properties. The NEMO-3 experiment [25] is proposed to investigate double beta decay processes with a sensitivity up to about 10^{25} yr. Its great advantage is related to the fact that the double beta emitters are part of the detectors themselves. This experiment can be also proposed to investigate the nuclear response for supernova neutrino spectra. In the present paper we focus on ^{82}Se isotope, which is about 1 kg in the source foil of the NEMO-3 detector (see Table 1 of Ref. [25]).

Various nuclear structure models have been employed to provide nuclear transition matrix elements and among them the quasi-particle random phase approximation (QRPA) is offering reliable neutrino–nucleus reactions cross-sections needed for current neutrino detection experiments and star evolution modelling. Its main advantage lies in the ability to provide calculations based on a very large valence space. In the present work, the dependence of the differential and integrated cross-sections of neutral current reaction $^{82}\text{Se}(\nu, \nu')^{82}\text{Se}^*$ on the scattering angle and initial neutrino-energy, is investigated using QRPA. Our code permits the evaluation of the individual contribution of the various incoherent (inelastic) neutrino induced nuclear transitions. The corresponding reduced matrix elements in the low and intermediate neutrino energy range have been calculated utilizing the method of Refs. [20–24].

2. Nuclear responses for supernova neutrinos

Nuclear responses for neutrinos are of vital importance for neutrino studies by means of nuclear weak processes. Neutrinos to be well studied in nuclei are low-energy neutrinos with energy $\epsilon_\nu = 0.1\text{--}50$ MeV. This is just the nuclear excitation region where Gamow–Teller (GT) and Fermi giant resonances as well as isospin and spin–isospin dipole resonances, play crucial role for nuclear responses [26].

Isospin and spin–isospin giant resonances, which absorb most of isospin and spin–isospin strengths, are located at the excitation region of $E_{\text{ex}} = 10\text{--}30$ MeV. Giant resonances associated with the weak processes are IAR (isobaric analogue resonance), GTR (GT giant resonance), IDR (isospin dipole resonance) and ISDR (isospin–spin dipole resonance). IAR and GTR are associated with Fermi-type isospin and GT-type spin-isospin transitions with $\Delta L = 0$, and IDR and ISDR with isospin and spin-isospin dipole transitions with $\Delta L = 1$, respectively [26].

On the other hand, isospin and spin–isospin strengths for low-lying states are reduced much because of destructive interference with the high-lying giant resonances. Consequently, nuclear responses for neutrinos with energy $\epsilon_\nu \leq 3\text{--}5$ MeV are small.

3. Brief description of the formalism

In the present work we consider neutral current neutrino–nucleus interactions in which a low or intermediate energy neutrino (or antineutrino) is scattered inelastically from a nucleus (A, Z). The initial nucleus is assumed to be spherically symmetric having ground state a $J^\pi = 0^+$ state.

The corresponding standard model effective Hamiltonian in current–current interaction form is written as

$$\mathcal{H} = \frac{G}{\sqrt{2}} j_\mu(\mathbf{x}) J^\mu(\mathbf{x}), \quad (3)$$

where $G = 1.1664 \times 10^{-5}$ GeV $^{-2}$ is the Fermi weak coupling constant. j_μ and J^μ denote the leptonic and hadronic currents, respectively. According to V–A theory, the leptonic current takes the form

$$j_\mu = \bar{\psi}_{\nu_\ell}(x) \gamma_\mu (1 - \gamma_5) \psi_{\nu_\ell}(x), \quad (4)$$

where ψ_{ν_ℓ} are the neutrino/antineutrino spinors.

From a nuclear physics point of view only the hadronic current is important. The structure for neutral current processes of both vector and axial-vector components (neglecting the pseudo-scalar contributions) is written as

$$J_\mu = \bar{\Psi}_N \left[F_1 \gamma_\mu + F_2 \frac{i\sigma_{\mu\nu} q^\nu}{2M} + F_A \gamma_\mu \gamma_5 \right] \Psi_N \quad (5)$$

(M stands for the nucleon mass and Ψ_N denote the nucleon spinors). F_i , $i = 1, 2$ represent the weak nucleon form factors given in terms of the well known charge and electromagnetic form factors (CVC-theory) for proton (F_i^p) and neutron (F_i^n) by the expressions [27]

$$F_{1,2} = \left(\frac{1}{2} - \sin^2 \theta_W \right) \left[F_{1,2}^p - F_{1,2}^n \right] \tau_0 - \sin^2 \theta_W \left[F_{1,2}^p + F_{1,2}^n \right]. \quad (6)$$

Here τ_0 represents the nucleon isospin operator and θ_W is the Weinberg angle ($\sin^2 \theta_W = 0.2325$). In Eq. (5) F_A stands for the axial-vector form factor for which we employ the dipole ansatz given by

$$F_A = -\frac{1}{2}g_A \left(1 - \frac{q^2}{M_A^2}\right)^{-2} \tau_0, \tag{7}$$

where $M_A = 1.05 \text{ GeV}$, is the dipole mass, and $g_A = 1.258$, is the static value (at $q = 0$) of the axial form factor.

In the convention we used in the present work q^2 , the square of the momentum transfer, is written as

$$q^2 = q^\mu q_\mu = \omega^2 - \mathbf{q}^2 = (\varepsilon_i - \varepsilon_f)^2 - (\mathbf{p}_i - \mathbf{p}_f)^2, \tag{8}$$

where $\omega = \varepsilon_i - \varepsilon_f$ is the excitation energy of the nucleus. ε_i denotes the energy of the incoming and ε_f that of the outgoing neutrino. $\mathbf{p}_i, \mathbf{p}_f$ are the corresponding 3-momenta of the incoming and outgoing neutrino/antineutrino, respectively. In Eq. (6) we have not taken into account the strange quark contributions in the form factors. In the scattering reaction considered in this work only low-momentum transfers are involved and the contributions from strangeness can be neglected [28].

The neutral-current neutrino/antineutrino–nucleus differential cross-section, after applying a multipole analysis of the weak hadronic current as in [29], is written as

$$\left(\frac{d^2\sigma_{i \rightarrow f}}{d\theta d\omega}\right)_{\nu/\bar{\nu}} = \frac{G^2}{\pi} \frac{|\vec{p}_f| \varepsilon_f}{(2J_i + 1)} \left(\sum_{J=0}^{\infty} \sigma_{\text{CL}}^J + \sum_{J=1}^{\infty} \sigma_{\text{T}}^J \right), \tag{9}$$

θ denotes the lepton scattering angle. The summations in Eq. (9) contain the contributions σ_{CL}^J , for the Coulomb $\widehat{\mathcal{M}}_J$ and longitudinal $\widehat{\mathcal{L}}_J$, and σ_{T}^J , for the transverse electric $\widehat{\mathcal{T}}_J^{\text{el}}$ and magnetic $\widehat{\mathcal{T}}_J^{\text{mag}}$ multipole operators defined as in Ref. [30]. These operators include both polar-vector and axial-vector weak interaction components. The contributions σ_{CL}^J , and σ_{T}^J are

$$\begin{aligned} \sigma_{\text{CL}}^J &= (1 + \cos \theta) \left| \langle J_f || \widehat{\mathcal{M}}_J(q) || J_i \rangle \right|^2 + (1 + \cos \theta - 2b \sin^2 \theta) \left| \langle J_f || \widehat{\mathcal{L}}_J(q) || J_i \rangle \right|^2 \\ &+ \left[\frac{\omega}{q} (1 + \cos \theta) \right] 2\text{Re} \, e \langle J_f || \widehat{\mathcal{L}}_J(q) || J_i \rangle \langle J_f || \widehat{\mathcal{M}}_J(q) || J_i \rangle^*, \end{aligned} \tag{10}$$

$$\begin{aligned} \sigma_{\text{T}}^J &= (1 - \cos \theta + b \sin^2 \theta) \left[\left| \langle J_f || \widehat{\mathcal{T}}_J^{\text{mag}}(q) || J_i \rangle \right|^2 + \left| \langle J_f || \widehat{\mathcal{T}}_J^{\text{el}}(q) || J_i \rangle \right|^2 \right] \\ &\mp \frac{(\varepsilon_i + \varepsilon_f)}{q} (1 - \cos \theta) 2\text{Re} \, e \langle J_f || \widehat{\mathcal{T}}_J^{\text{mag}}(q) || J_i \rangle \langle J_f || \widehat{\mathcal{T}}_J^{\text{el}}(q) || J_i \rangle^*, \end{aligned} \tag{11}$$

where $b = \varepsilon_i \varepsilon_f / q^2$.

4. Results

4.1. Calculated cross-sections

In order to investigate neutrino scattering off the ^{82}Se nucleus we performed explicit state-by-state calculations for the nuclear transition matrix elements within the QRPA. The initial nucleus was assumed to be spherically symmetric (having a 0^+ ground state). We adopted the full $3\hbar\omega$ and $4\hbar\omega$ model space for both protons and neutrons considering elementary excitations of one-particle–one-hole (1p–1h) type. The corresponding single particle energies (s.p.e) were produced by a Coulomb corrected Woods–Saxon potential using the parameters of Bohr and Mottelson [32].

The two-body interaction matrix elements were obtained from the Bonn one-boson-exchange potential applying G -matrix techniques [33]. The strong pairing interaction between the nucleons can be adjusted by solving the BCS equations. The monopole matrix elements of the two-body interaction are scaled by the pairing-strength parameters g_{pair}^p and g_{pair}^n separately for protons and neutrons. The adjustment can be done by comparing the resulting lowest quasiparticle energy to reproduce the phenomenological pairing gap obtained by using the linear approximation [34, 35]

$$\Delta_n({}^A_Z X) = -\frac{1}{4} \left[S_n({}^{A+1}_Z X) - 2S_n({}^A_Z X) + S_n({}^{A-1}_Z X) \right], \quad (12)$$

$$\Delta_p({}^A_Z X) = -\frac{1}{4} \left[S_p({}^{A+1}_{Z+1} X) - 2S_p({}^A_Z X) + S_p({}^{A-1}_{Z-1} X) \right], \quad (13)$$

in which ${}^A_Z X$ stands for the doubly-even nucleus under consideration. The separation energies $S_{n/p}$ are provided, *e.g.*, by [36]. The results of this procedure lead to the pairing-strength parameters $g_{\text{pair}}^p = 0.92$ and $g_{\text{pair}}^n = 1.24$.

After settling the values of the pairing parameters, two other parameters are left to fix, the overall scale of the particle–hole interaction g_{ph} and separately the particle–particle channel of the interaction g_{pp} for each multipole up to $J = 8^\pm$. In the present work we fixed the QRPA parameters on the bound energy spectrum, so as the low-lying excitation energies to fit the experimental spectrum [20–24]. An alternative fixing of the parameters g_{ph} and g_{pp} , especially for the charged-current neutrino–nucleus reactions, could be done on the giant dipole resonance of the studied nucleus.

We found that the excitation energies were almost independent on the g_{pp} parameter so that the same value $g_{\text{pp}} = 1$ was adopted. This means that, during all the calculations, the particle–particle channel of the nucleon–nucleon interaction was not renormalized and corresponds to the bare G matrix of (finite-size) nuclear matter. Contrary to the unique value of the particle–particle strength, the particle–hole parameter g_{ph} varied within 30% of the value $g_{\text{ph}} = 1$. A feature which diminishes the arbitrariness of choosing

the value of g_{ph} is that this parameter only affects the lowest collective-like excitation, leaving the other states nearly unaffected. This means that the predictions for the vast majority of the states are virtually parameter-independent and thus are truly microscopic predictions depending solely on the model space, the description of the pairing properties of the nucleons, the truncation scheme of the nuclear excitation theory as well as the global features of the nucleon–nucleon interaction. It should be noted that the ground-state correlations (spurious effects due to broken symmetries) [35] have not been taken into account.

In the following we proceed with the calculation of the cross-sections, for neutrino energies $\epsilon_i \leq 100$ MeV. After obtaining the double differential cross-section $d^2\sigma/d\theta d\epsilon_i$, the single differential cross-section $d\sigma/d\omega$, is calculated by summing over partial rates of all multipole states up to $J = 8^\pm$. Figure 2 shows the double differential cross-section *versus* initial neutrino energy for various scattering angle θ (step $\Delta\theta = 15^\circ$ from $\theta = 0^\circ$ to $\theta = 165^\circ$). In general, our results show a smooth dependence of $d^2\sigma/d\theta d\epsilon_i$ on the initial neutrino energy, ϵ_i . As can be seen, for low neutrino energies up to about $\epsilon_i \leq 8\text{--}12$ MeV, namely for the region of the discrete energy spectrum of ^{82}Se , the differential cross-section decreases as the scattering angle increases but for higher energies the trend is reversed. This effect is due to the dominance of the transverse contribution as the scattering angle increases and reminds us the similar behavior occurring in inelastic electron scattering.

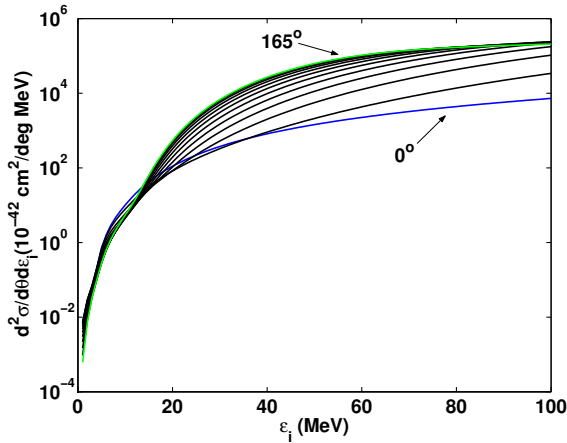


Fig. 2. Double differential cross-section $d^2\sigma/d\theta d\epsilon_i$ for the reaction $^{82}\text{Se}(\nu, \nu')^{82}\text{Se}^*$ as a function of the neutrino energy and the scattering direction of the lepton. The single differential cross-section $d\sigma/d\omega$ were obtained by summing over partial rates for the various sets of multipole states up to $J = 8^\pm$. Results are given for scattering angles between $\theta = 0^\circ$ to $\theta = 165^\circ$, in 15° steps.

The contribution of the dominant multipole states up to $J = 8^\pm$ to the differential cross-section, $d\sigma/d\omega$, is illustrated in Fig. 3 for some characteristic impinging neutrino energies $\epsilon_i = 15, 30, 50$ MeV. When $\epsilon_i = 15$ MeV,

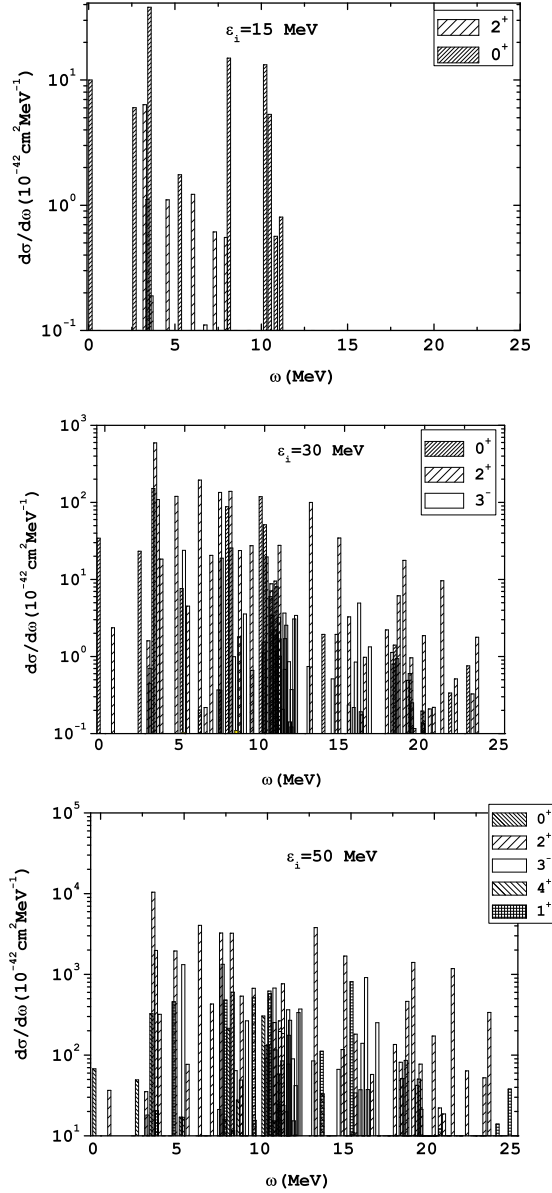


Fig. 3. Contribution of the different multipolarities to the differential cross-section, $d\sigma/d\omega$, with respect to the excitation energy ω , at the incoming neutrino energy $\epsilon_i = 15, 30$ and 50 MeV.

$d\sigma/d\omega$ (Fig. 3 top) is dominated by the transitions to the multipole states $J = 0^+$ and 2^+ . As the neutrino energy increases to $\epsilon_i = 30$ MeV transitions to $J = 3^-$ start to contribute significantly (Fig. 3 middle). Finally, when $\epsilon_i = 50$ MeV other multipolarities such as $J = 1^+$ and $J = 4^+$ start to play a significant role (Fig. 3 bottom). Consequently, as the neutrino energy increases the cross-section is being spread among other multipolarities.

Figure 4 shows the dependence of the integrated cross-section $\sigma(\epsilon_i)$ on the incoming neutrino energy ϵ_i . Our results were obtained from the double differential cross-section by summing over all possible final nuclear states and by numerical integration over angles. The general trend is that the cross-section is proportional to the square of the lepton energy. The individual contributions of the polar vector and axial vector components of the current are also shown in the same figure. It is worth mentioning that for energies greater than $\epsilon_i \geq 15$ MeV the cross-section comes from the axial vector component of the operator.

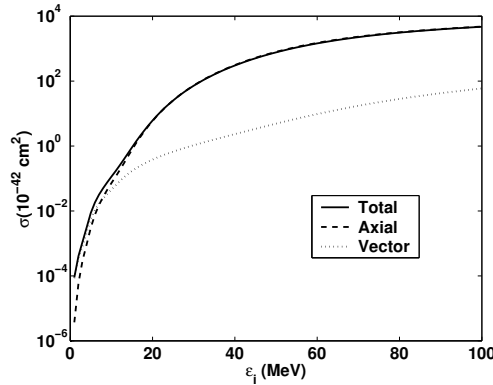


Fig. 4. Individual contributions coming from vector and axial-vector components. The full line gives the integrated cross-section, the dash-dotted the axial contribution and the dotted line the vector one.

Table I presents our results for the integrated cross-sections for the reaction $^{82}\text{Se}(\nu, \nu')^{82}\text{Se}^*$. The range of the incoming neutrino energies is $5 \leq \epsilon_i \leq 100$ MeV. For comparison the integrated total cross-sections of $^{56}\text{Fe}(\nu, \nu')^{56}\text{Fe}^*$ obtained by our QRPA model (third column) and those obtained by Kolbe and Langanke [18] (forth column) are included. It should be noted that results of Ref. [18] have been obtained by a hybrid approach that combines Shell Model calculations and Continuum RPA. As can be seen, our total cross-sections (in 10^{-42} cm^2) are in good agreement with those of Ref. [18] (for neutrino energy less than 10 MeV there are no results of Ref. [18] to compare with). Some differences of at most 50% at low neutrino energies may be attributed to different theoretical approaches as well

TABLE I

Integrated cross-sections (in 10^{-42} cm^2) for neutral-current neutrino–nucleus reaction $^{82}\text{Se}(\nu, \nu')^{82}\text{Se}^*$ calculated with the QRPA method. The exponents are given in parentheses. We also present the integrated cross-sections for the reaction $^{56}\text{Fe}(\nu, \nu')^{56}\text{Fe}^*$, calculated by our QRPA model [20] (third column) and by Kolbe and Langanke [18] (forth column).

Initial energy of incoming ν ϵ_i [MeV]	^{82}Se	^{56}Fe [20]	^{56}Fe [18]
5	1.01(−2)	—	—
10	1.13(−1)	1.01(+0)	1.91(−1)
15	9.03(−1)	2.85(+0)	2.19(+0)
20	6.09(+0)	5.79(+0)	6.90(+0)
25	2.52(+1)	1.06(+1)	1.51(+1)
30	7.19(+1)	1.87(+1)	2.85(+1)
35	1.60(+2)	3.24(+1)	4.89(+1)
40	3.01(+2)	5.51(+1)	7.86(+1)
45	5.03(+2)	9.05(+1)	1.19(+2)
50	7.65(+2)	1.43(+2)	1.72(+2)
55	1.08(+3)	2.15(+2)	2.39(+2)
60	1.44(+3)	3.09(+2)	3.20(+2)
65	1.84(+3)	4.26(+2)	4.15(+2)
70	2.26(+3)	5.63(+2)	5.25(+2)
75	2.68(+3)	7.17(+2)	6.50(+2)
80	3.10(+3)	8.82(+2)	7.89(+2)
85	3.52(+3)	1.05(+3)	9.42(+2)
90	3.92(+3)	1.22(+3)	1.11(+3)
95	4.32(+3)	1.38(+3)	1.29(+3)
100	4.70(+3)	1.52(+3)	1.49(+3)

as to different parametrization in single particle energies and effective interaction. Obviously, various theoretical approaches differ in the predicted neutrino–nucleus cross-sections and this will require more detailed studies of the underlying nuclear structure that contributes to the neutrino reaction rates. On the other hand, the only experimental data for $^{56}\text{Fe}(\nu, \nu')^{56}\text{Fe}^*$ reaction are from KARMEN Collaboration [37] and this result has yet to be confirmed by independent measurements.

4.2. The folding procedure

In order to obtain more information about supernova neutrinos, the integrated cross-section $\sigma(\epsilon_i)$ has to be folded with the appropriate energy distribution. Refs. [38, 39] advocate Fermi–Dirac spectra with temperatures around 8 to 10 MeV for heavy flavor neutrinos not taking part in charged-current reactions, and decoupling closer to the center of the supernova,

5 MeV for electron antineutrinos, and even slightly lower values for electron neutrinos interacting with the larger number of neutrons in the star core. The shape of the spectrum is most accurately described when a chemical potential is included. The energy distribution is then given by

$$n_i(\epsilon_i, T, \alpha) = \frac{N_2(\alpha)}{T^3} \frac{\epsilon_i^2}{1 + \exp[(\epsilon_i/T) + \alpha]}, \tag{14}$$

where T is the neutrino temperature and α parameter associated with the non-zero chemical potential μ

$$\alpha = \frac{\mu}{T}, \tag{15}$$

$N_2(\alpha)$ denotes the normalization factor depending on α given from

$$N_k(\alpha) = \left(\int_0^\infty \frac{x^k}{1 + e^{x-\alpha}} dx \right)^{-1}, \tag{16}$$

for $k = 2$. Following Ref. [40], the average neutrino energy $\langle \epsilon_i \rangle$ can be written in terms of the functions of Eq. (16) as

$$\langle \epsilon_i \rangle = \frac{N_2(\alpha)}{N_3(\alpha)} T. \tag{17}$$

The flux-averaged total cross-section can be calculated by convoluting the inclusive integrated cross-section of Fig. 4 by a Fermi–Dirac spectrum [41–43]:

$$\langle \sigma \rangle = \int_0^\infty \sigma(\epsilon_i) n_i(\epsilon_i, T, \alpha) d\epsilon_i. \tag{18}$$

Figure 5 shows the averaged neutrino energy as a function of the parameter α for various temperatures T . As it is seen the introduction of a chemical potential in the spectrum at fixed neutrino temperature increases the average neutrino energy.

Figure 6 illustrates the temperature dependence of the flux-averaged total cross-section for a variety of neutrino-energy distributions. With increasing temperature a broadening of the spectrum emerges, and a shift of the neutrino energies to higher values is observed. This explains the steep rise in the cross-section when the spectrum temperature is going up. Not only the average neutrino energy is rising, but also relatively more high-energy neutrinos are contributing. As we mentioned the introduction of a chemical

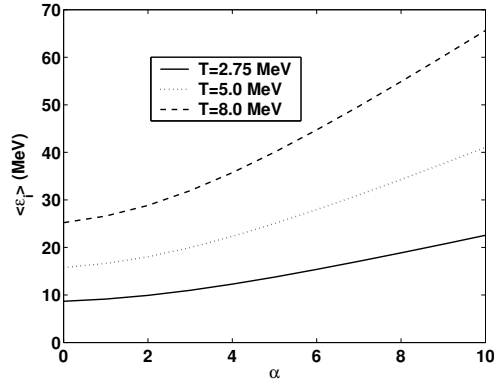


Fig. 5. Averaged neutrino energy as a function of the parameter α for various temperatures T .

potential in a spectrum at fixed neutrino temperature increases the average neutrino energy. This is clearly reflected in Fig. 6; at fixed neutrino temperature a non vanishing chemical potential enhances the cross-section. On the other hand, the inclination of the blue solid lines linking spectra with equal average neutrino energies shows that for distributions with the same average energy, spectra with a higher chemical potential result in smaller cross-sections. This is easily explained by the observation that due to the depletion of the high energy part of the spectrum, less high energy neutrinos will be arriving, reducing the response in a terrestrial detector accordingly.

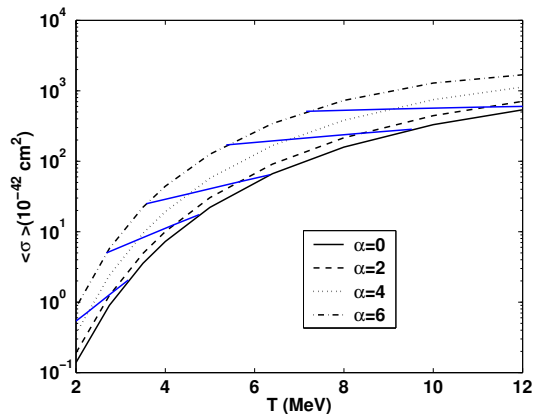


Fig. 6. Flux-averaged total cross-section for neutral-current neutrino scattering on $^{82}\text{Se}(\nu, \nu')^{82}\text{Se}^*$, folded with a Fermi–Dirac spectrum as a function of the temperature T and the chemical potential of the neutrino energy distribution. The straight solid lines connect spectra with the same average energy.

Finally, Table II shows the flux-averaged total cross-section at some interesting neutrino temperatures T obtained by using the two parameter Fermi–Dirac neutrino-energy distribution. The chemical potential parameters $a = 0$ and $a = 3$ have been used in order to describe the supernovae spectrum [39]. The relative results for ^{56}Fe and ^{208}Pb isotopes obtained previously [18, 42] are also included. As it is seen, the calculated flux-averaged total neutral-current cross-sections for ^{82}Se are more close to those of ^{56}Fe at low neutrino temperatures and more close to those of ^{208}Pb at higher neutrino temperatures.

TABLE II

Flux-averaged total cross-section $\langle\sigma\rangle$ (in 10^{-42} cm 2) for neutral-current scattering on ^{82}Se corresponding to supernova neutrino spectra described by a two parameter Fermi–Dirac distribution with $\alpha = 0$ and 3, for various temperatures T (MeV). In this table we also list the results for ^{56}Fe and ^{208}Pb isotopes, studied previously [18, 42]. For comparison the cross-sections are averaged over neutrinos and antineutrinos.

(T, α)	(2.75,0)	(4,0)	(6,0)	(8,0)	(10,0)	(2.75,3)	(3,3)	(4,3)	(6.26,3)
^{56}Fe	1	3.7	16	43	90	1	2.1	6.4	32
^{82}Se	0.9	7.6	50	158	330	1.7	2.7	13	109
^{208}Pb	—	14	62	160	330	—	8.1	25	120

5. Conclusions

In the present paper we employed the quasi-particle random phase approximation to study neutral current neutrino–nucleus inelastic scattering cross-sections concerning ^{82}Se nucleus. Our model was tested so that the low lying energy spectrum can be reproduced. The dependence of the cross-sections on the scattering angle θ and initial neutrino energy is investigated for both Fermi and Gamow–Teller like operators. It is revealed that, as the neutrino energy increases, the differential cross-section $d\sigma/d\omega$ is being spread over many multipolarities. The major multipole contributions stem from $J^\pi = 0^+, 1^+, 2^+, 4^+$ and $J^\pi = 3^-$. Moreover, the double differential cross-section decreases as the scattering angle increases in the neutrino energy range $\epsilon_i \leq 8\text{--}12$ MeV but for higher energies the cross-section increases with the scattering angle. Comparing the contribution of the individual vector component with the axial vector one we found that for energies $\epsilon_i \geq 15$ MeV, the integrated cross-section comes from the axial vector component. This means that for solar neutrino detection only the vector component participates in the detection signal. The flux-averaged total cross-sections of ^{82}Se were obtained for several parameters of the Fermi–Dirac neutrino-energy

distributions. Such results describe the response of the studied isotope as supernova neutrino detector. It should be noticed that ^{82}Se -isotope is a target, among other isotopes like Cd and Mo, of recent experiments (NEMO, MOON, COBRA *etc.*), which are currently used for searches on the neutrinoless double beta decay and direct detection of cold dark matter (CDM) particles.

REFERENCES

- [1] T.W. Donnelly, R.D. Peccei, *Phys. Rep.* **50**, 1 (1979).
- [2] R. Davis, *Prog. Part. Nucl. Phys.* **32**, 13 (1994).
- [3] E. Kolbe, T.S. Kosmas, *Springer Trac. Mod. Phys.* **163**, 199 (2000) and references therein.
- [4] W.C. Haxton, *Phys. Rev. Lett.* **60**, 768 (1988).
- [5] J.N. Bahcall, R.K. Ulrich, *Rev. Mod. Phys.* **60**, 297 (1988); K. Kubodera, S. Nozawa, *Int. J. Mod. Phys.* **E3**, 101 (1994).
- [6] J. Rapaport *et al.*, *Phys. Rev. Lett.* **47**, 1518 (1981); **54**, 2325 (1985); D. Krofcheck *et al.*, *Phys. Rev. Lett.* **55**, 1051 (1985); *Phys. Lett.* **B189**, 299 (1987); Yu.S. Lutostansky, N.B. Skul'gina, *Phys. Rev. Lett.* **67**, 430 (1991).
- [7] J.W.F. Valle, [hep-ph/0610247](https://arxiv.org/abs/hep-ph/0610247) and references therein.
- [8] [KARMEN Collaboration] B. Bodmann *et al.*, *Phys. Lett.* **B267**, 321 (1991); **B280**, 198 (1992); **B332**, 251 (1994).
- [9] G. Drexlin *et al.*, *Prog. Part. Nucl. Phys.* **32**, 375 (1994).
- [10] C. Volpe, *et. al.*, *Phys. Rev.* **C65**, 044603 (2002).
- [11] T.W. Donnelly, J.D. Walecka, *Phys. Lett.* **B41**, 275 (1972); T.W. Donnelly, *Phys. Lett.* **B43**, 93 (1973); J.B. Langworthy, B.A. Lamers, H. Uberall, *Nucl. Phys.* **A280**, 351 (1977); E.V. Bugaev *et al.*, *Nucl. Phys.* **A324**, 350 (1979).
- [12] J.S. Bell, C.H. Llewellyn-Smith, *Nucl. Phys.* **B28**, 317 (1971).
- [13] T.K. Gaisser, J.S. O'Connell, *Phys. Rev.* **D34**, 822 (1986); T. Kuramoto, M. Fukugita, Y. Kohyama, K. Kubodera, *Nucl. Phys.* **A512**, 711 (1990).
- [14] S.K. Singh, E. Oset, *Nucl. Phys.* **A542**, 587 (1992).
- [15] E. Kolbe, *Phys. Rev.* **C54**, 1741 (1996).
- [16] T.S. Kosmas, E. Oset, *Phys. Rev.* **C53**, 1409 (1996).
- [17] P.C. Divari, T.S. Kosmas, J.D. Vergados, L.D. Skouras, *Phys. Rev.* **C61**, 054612 (2000).
- [18] E. Kolbe, K. Langanke, *Phys. Rev.* **C63**, 025802 (2001).
- [19] N. Jachowicz, K. Heyde, S. Rombouts, *Nucl. Phys.* **A688**, 593 (2001).
- [20] V.Ch. Chasioti, T.S. Kosmas, P.C. Divari, *Prog. Part. Nucl. Phys.* **59**, 481 (2007).
- [21] V. Tsakstara, T.S. Kosmas, P.C. Divari, J. Sinatkas, *Prog. Part. Nucl. Phys.* in press, doi:10.1016/j.pnpnp.2009.12.061.

- [22] K.G. Balasi, T.S. Kosmas, P.C. Divari, *Prog. Part. Nucl. Phys.* in press, doi:10.1016/j.pnpnp.2009.12.062.
- [23] V. Tsakstara, T.S. Kosmas, P.C. Divari, *J. Phys.: Conf. Ser.* **203**, 012101 (2010); V. Tsakstara, T.S. Kosmas, P.C. Divari, J. Sinatkas, *AIP Conf. Proc.* **1180**, 140 (2009); T.S. Kosmas, V. Tsakstara, P.C. Divari, J. Sinatkas, *AIP Conf. Proc.* **1180**, 61 (2009); K.G. Balasi, T.S. Kosmas, P.C. Divari, V.Ch. Chasioti, *AIP Conf. Proc.* **972**, 554 (2008).
- [24] V.Ch. Chasioti, T.S. Kosmas, *Nucl. Phys.* **A829**, 234 (2009).
- [25] A.S. Barabash, *Phys. Atom. Nucl.* **68**, 414 (2005); F. Mauger, *J. Phys.: Conf. Ser.* **203**, 012065 (2010).
- [26] H. Ejiri, *Phys. Rep.* **338**, 265 (2000) and references therein.
- [27] M.S. Athar, S. Ahmad, S.K. Singh, *Nucl. Phys.* **A694**, 551 (2006).
- [28] A. Meucci, C. Giusti, F.D. Pacati, *Nucl. Phys.* **A744**, 307 (2004).
- [29] T.W. Donnelly, J.D. Walecka, *Nucl. Phys.* **A201**, 81 (1973).
- [30] E. Kolbe, K. Langanke, P. Vogel, *Phys. Rev.* **D66**, 013007 (2002).
- [31] O. Civitarese, A. Faessler, T. Tomoda, *Phys. Lett.* **B194**, 11 (1987).
- [32] A. Bohr, B.R. Mottelson, *Nucl. Struct.*, Vol. 1, Benjamin, New York 1969.
- [33] K. Holinde, *Phys. Rep.* **68**, 121 (1981).
- [34] W.A. Kaminski, A. Faessler, *Nucl. Phys.* **A529**, 605 (1991).
- [35] T.S. Kosmas, *Nucl. Phys.* **A683**, 443 (2001).
- [36] G. Audi *et al.* *Nucl. Phys.* **A729**, 337 (2003).
- [37] R. Maschuw, *Prog. Part. Nucl. Phys.* **40**, 183 (1998).
- [38] H.-T. Janka, W. Hillebrandt, *Astron. Astrophys.* **78**, 373 (1998).
- [39] H.-T. Janka, W. Hillebrandt, *Astron. Astrophys.* **224**, 49 (1998).
- [40] M.S. Athar, S. Ahmad, S.K. Singh, *Phys. Rev.* **C71**, 045501 (2005).
- [41] N. Jachowicz, S. Rombouts, J. Ryckebusch, *Phys. Rev.* **C59**, 6 (1999).
- [42] J. Toivanen, E. Kolbe, K. Langanke, G. Martinez-Pinedo, P. Vogel, *Nucl. Phys.* **A694**, 395 (2001).
- [43] J.D. Vergados, H. Ejiri, *Nucl. Phys.* **B804**, 144 (2008).